View metadata, citation and similar papers at core.ac.uk

brought to you by CORE

provided by IntechOpen

We are IntechOpen, the world's leading publisher of Open Access books Built by scientists, for scientists

4,800
Open access books available

122,000
International authors and editors

135M
Downloads

Our authors are among the

154
Countries delivered to

TOP 1%
most cited scientists

12.2%
Contributors from top 500 universities

CLARIVATE ANALYTICS BOOK CITATION INDEX INDEXED

WEB OF SCIENCE™

Selection of our books indexed in the Book Citation Index in Web of Science™ Core Collection (BKCI)

Interested in publishing with us?
Contact book.department@intechopen.com

Numbers displayed above are based on latest data collected.
For more information visit www.intechopen.com

11

Design and Modeling of Microstrip Line to Substrate Integrated Waveguide Transitions

Ting-Yi Huang, Tze-Min Shen and Ruey-Beei Wu
National Taiwan University
Taiwan, R.O.C.

1. Introduction

Microstrip lines (MSL) are widely used in microwave systems because of its low cost, light weight, and easy integration with other components. Substrate integrated waveguides (SIW), which inherit the advantages from traditional rectangular waveguides without their bulky configuration, aroused recently in low loss and high power planar applications. This chapter proposed the design and modeling of transitions between these two common structures. Research motives will be described firstly in the next subsection, followed by a literature survey on the proposed MSL to SIW transition structures. Outlines of the following sections in this chapter will also be given in the end of this section.

1.1 Research Motives

Planar transmission lines, such as MSL and coplanar waveguides (CPW), are favorable in the integration of microwave systems. For low loss and high power applications, rectangular waveguides are often used for signal transmission between system modules. A vast of transition structures between planar circuits and rectangular waveguides have also been proposed, e.g., [Das et al., 1986; Kaneda et al., 1999; Lin & Wu, 2001]. However, systems with rectangular waveguides are often large and heavy. Transitions between rectangular waveguides and planar circuits cannot be held without extra supporting structures. Recently, SIWs were proposed as a replacement for miniaturized and light weighted applications. Nonetheless, such transitions can shed some light on the design of MSL to SIW transitions.

SIW, as its name, can be easily integrated into the substrates of planar circuits, such as printed circuit boards (PCB) and low temperature co-fired ceramics (LTCC), with their standard fabrication processes. Compared with conventional rectangular waveguides, SIW has the advantage of low-cost, compact, and easy-integration with planar circuits. Although their quality factors cannot compete with those of traditional rectangular waveguides, they are more suitable in system integration.

For system using both MSL and SIW, LTCC is often preferred for its multilayer nature and three-dimensional interconnection capability. System on package (SOP) modules can be fabricated on LTCC with various passive elements embedded. Therefore the required circuit

area can be reduced significantly. This chapter aims at design and modeling of the transitions structures between MSL and SIW on LTCC substrate for better transition performance and wider bandwidth.

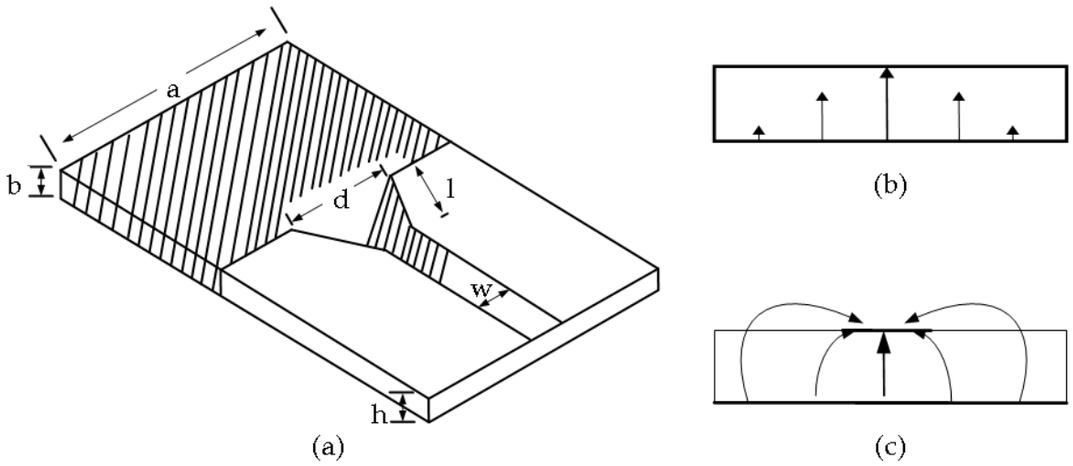

Fig. 1. MSL to SIW transition with tapered microstrip feeding. (a) Transition structure. (b) Electric field distribution in SIW cross section. (c) Electric field distribution in MSL cross section [Deslandes & Wu, 2001a].

1.2 Literature Survey

Transition structures between planar circuits and traditional rectangular waveguides have been widely studied and many high performance transitions are proposed. However, complicated structures are required to hold or support the transitions and precise fabrication processes are also needed at millimeter wave frequencies. Many of these structures can be adopted for the transitions between planar circuits and SIW directly or with little modification, but with lower cost and more reliable fabrication process. On the other hand, since planar circuits and SIW can be integrated on the same substrate, much simpler structures are able to accomplish the transition and many of them have been proposed and demonstrated with good performance.

Tapered microstrip feeding [Deslandes & Wu, 2001a] is commonly used in the transition between MSL and SIW. As shown in Fig. 1a, a MSL is connected directly to the top wall of SIW through a tapered microstrip section. The vertical components of electric field in both MSL and SIW regions are well matched, as shown in Fig. 1b and Fig. 1c, therefore the transition can be easily achieved. However, in order to reduce the discontinuity effect, a long enough tapered microstrip section is needed, up to a half wavelength in some cases. Another disadvantage of this transition structure requires the MSL on the same layer where the metal wall of SIW is located. Also, the MSL is directly connected to SIW. DC current from MSL will be shorted into ground through SIW. Transition by direct connection can also be found between CPW and SIW [Deslandes & Wu, 2001b]. As other direct connected transition structures, additional DC blocking circuit is needed because the signal line is shorted to the ground. For thick substrates, extra insertion loss may be introduced due to slot radiation.

Transition by probe feeding is often used between coaxial lines and traditional rectangular waveguides, e.g., [Collins, 1991; Liang et al., 1992; Rollins & Jarem, 1989]. MSL can also achieve probe feeding [Shih et al., 1998] by shorting its ground plane to one of the longer edge of the waveguide and stretch its signal line into the waveguide. By properly designing the stretching length, the feeding position, and the quarter wavelength transformer for impedance matching, about 40% fractional bandwidth can be achieved.

In multilayer substrates, modified probe feeding can be used for the transition between MSL and SIW. A V-band MSL to SIW transition in LTCC is proposed [Huang et al., 2003]. MSL is shorted to the bottom wall of SIW with a through hole via, which act as an excitation probe. Sizes of via pads between different layers are adjusted to achieve better impedance matching. Three different designs have also been investigated and their performances are compared [Kai et al., 2005]. However, it deserves mentioning that the thickness of SIW is much smaller than that of the metallic waveguide. Hence, the impedance matching is in general worse and will result in larger reflection. With some special compensation design, the transitions with relative bandwidth of about 10% have been reported.

A systematic design approach to enhance the bandwidth of the simple probe feeding structure has also been proposed by our group [Yau et al., 2007], as shown in Fig. 2. The feeding position is chosen to be a quarter of guided wavelength in SIW from its shorted end. Electromagnetic wave excited by via current propagates in –z direction will be in phase with that propagates in +z direction after reflection. Impedance matching can be achieved by adjusting the sizes of the via pad at MSL and the anti-pad at the top wall of SIW. Further discussions and design examples of this transition structure will be given in this chapter.

The DC shorting problem can be avoided if the transition is accomplished by coupling. Our group has also suggested the MSL to SIW transition by an open stripline stub [Yang et al., 2005]. MSL is connected to a stripline stub which stretch into the SIW for about a half wavelength. Impedance matching is done by adjusting the width of the MSL and stripline stub.

On the other hand, by opening a slot at the current return path of MSL, energy can be coupled to traditional rectangular waveguide [Grabherr et al., 1994]. By properly choosing the slot length and position, transition bandwidth can be enhanced. Transition by slot coupling can also be utilized between MSL and SIW, as shown in Fig. 3. By opening a thin slot on the common metal plane of MSL and SIW, energy can be coupled between these two structures through the slot. Transition bandwidth and frequency can be controlled by properly adjusting the lengths of the slot and the microstrip open stub. Open-type transitions often suffer from low bandwidth. In order to improve the transition bandwidth, detailed discussions and several design examples will also be presented in this chapter.

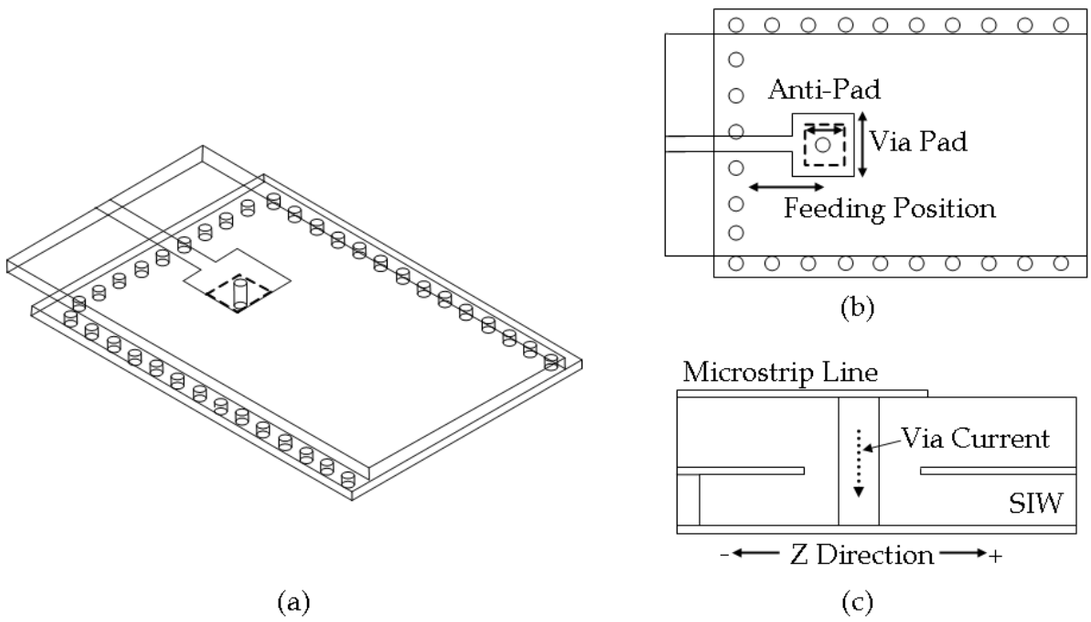

Fig. 2. MSL to SIW transition by probe feeding with via pad and anti-pad compensation. (a) 3D view. (b) Top view. (c) Side view.

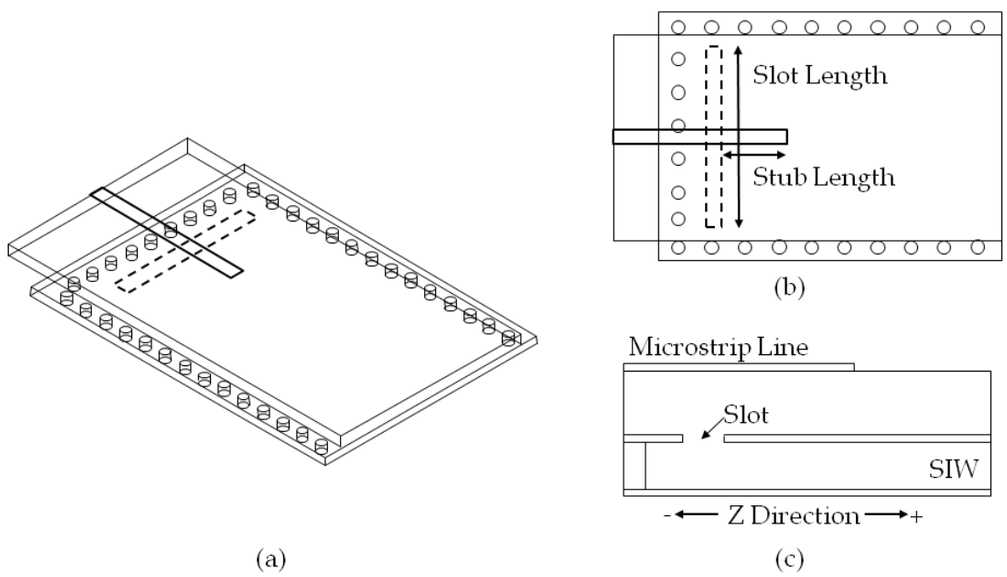

Fig. 3. MSL to SIW transition by slot coupling. (a) 3D view. (b) Top view. (c) Side view.

1.3 Section Outlines

Remaining sections of this chapter are arranged as follows. Theory of MSL to SIW transitions will be derived in section 2, including the modal analysis of SIW, calculation of input resistances for current excitation and slot coupling, and model construction with

calculated input resistances. Two different kinds of transition structures, probe feeding and slot coupling, will then be presented in the following two sections. Each of these two sections begins with input resistance derivation and equivalent circuit construction by the theory proposed in section 2. Several design examples for both structures will also be presented with comparison between simulations and measurements. A brief summary and discussion will be given in the end of this chapter.

2. Theory of MSL to SIW Transitions

Rectangular waveguides are widely used in microwave systems for its high power handling ability, low radiation loss as well as low electromagnetic interference (EMI) to other circuit components. However they are also known with disadvantages such as bulky volume, heavy weight, high cost, and difficult integration with planar circuits. In addition, high precision process is required at millimeter wave frequencies. As a result, mass production is difficult for systems with rectangular waveguides.

Laminated waveguides were first proposed in 1998 [Uchimura et al., 1998], where waveguides can be embedded in multilayer printed circuit boards with their side walls replaced by via fences. In 2001, concept of substrate integrated waveguides (SIW) was also proposed [Deslandes and Wu, 2001a; Deslandes and Wu, 2001b]. Waveguides embedded in single layer substrates are demonstrated with transitions to CPWs and MSLs. These kinds of waveguides can be easily integrated with other circuit components by a standard planar circuit fabrication process. Volume and weight are also significantly reduced.

The structure and characteristic of SIWs will be introduced firstly in this section, followed by two kinds of excitation structures and calculation of their input resistances. Construction of the equivalent circuit models where the input resistances are associated will also be presented.

2.1 Modal Analysis of SIW

Figure 4a shows the structure of an SIW, which is composed of the top and bottom metal planes of a substrate and two parallel via fences in the substrate. In order to replace the vertical metal walls, via pitch must be small enough. The vias must be shorted to both metal planes to provide vertical current paths, as shown in Fig. 4b, otherwise the propagation characteristics of SIW will be significantly degraded.

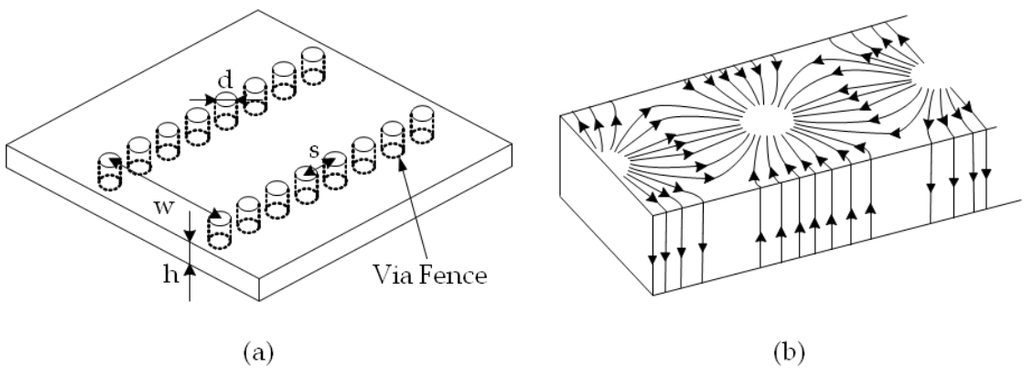

Fig. 4. (a) Structure of SIW and (b) surface current for TE_{10} mode.

Since the vertical metal walls are replaced by via fences for the SIW structures, propagating modes of SIW are very close to, but not exactly the same as, those of the rectangular waveguides. This can be verified by checking the modal surface current patterns. Only patterns with solely vertical current distributed on the side wall survive in SIWs. For example, Fig. 4b shows the TE_{10} mode surface current distribution of a rectangular waveguide. The current path will not be cut by the via fences, therefore TE_{10} mode can be supported in an SIW. This holds for all TE_{m0} modes since their current distributions on the side walls are similar. On the other hand, horizontal components of the surface current exist on the sidewalls for all TM modes and TE_{mn} modes with nonzero n's. These current paths will be cut in SIW structures, which results in radiation. Therefore we can conclude that only TE_{m0} modes exist in SIW structures. Properties of TE_{m0} modes are listed in Table 1 for later usage.

Property	**TE_{m0} modes**
Generating function	$\psi_{m0} = \cos m\pi x/a$
Cutoff wavenumber	$k_{c,m0} = m\pi/a$
Propagation constant	$\Gamma_{m0}^2 = k_{c,m0}^2 - k^2, \quad k = \omega\sqrt{\mu\varepsilon}$
Magnetic field	$\vec{H}_t = \pm\Gamma_{m0}\nabla_t \psi_{m0} e^{\pm\Gamma_{m0} z}, \quad H_{z,m0} = k_{c,m0}^2 \psi_{m0} e^{\pm\Gamma_{m0} z}$
Electric field	$\vec{E}_t = \pm Z_h \hat{a}_z \times \vec{H}_t, \quad Z_h = j\omega\mu_0/\Gamma = jk_0\eta/\Gamma$
Power flow	$ab\eta k\beta_{m0} k_{c,m0}^2/4$

Table 1. Properties of TE_{m0} modes.

2.2 Input Resistance of Current Excitation

For a waveguide excited by a current source along path C with current density J in the direction τ, as shown in Fig. 5, the magnitude and patterns of different modes excited can be calculated as follows.

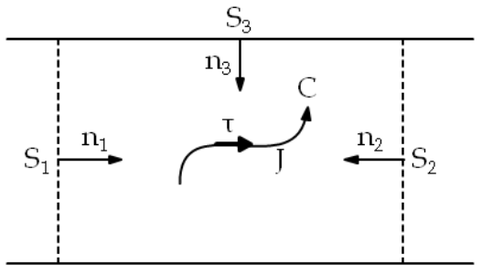

Fig. 5. Current excitation in a waveguide structure.

By the orthogonal property of waveguide modes, field propagating in the waveguide can be denoted by the linear combination of modal fields $\vec{E}_n^{\pm}$ and $\vec{H}_n^{\pm}$, which denote the electric and magnetic field of the n-th propagating mode along ±z direction, respectively. The field propagating along +z direction excited by the current can be decomposed as

$$\vec{E}^{+} = \sum_n a_n \vec{E}_n^{+}, \quad \vec{H}^{+} = \sum_n a_n \vec{H}_n^{+} \cdot \tag{1}$$

In the same manner, the field propagating along -z direction excited by the current can also be decomposed as

$$\vec{E}^{-} = \sum_n b_n \vec{E}_n^{-}, \quad \vec{H}^{-} = \sum_n b_n \vec{H}_n^{-} \cdot \tag{2}$$

Consider the region V enclosed by surfaces $S = S_1 + S_2 + S_3$. By reciprocity theorem [Harrington, 2001],

$$\oint_S \hat{n} \cdot \left(\vec{E}_n^{\pm} \times \vec{H} - \vec{E} \times \vec{H}_n^{\pm}\right) dS = \int_V \vec{J} \cdot \vec{E}_n^{\pm} \, dV \cdot \tag{3}$$

For $\vec{E}_n^{-}$ and $\vec{H}_n^{-}$ modes, (3) can be reduced into

$$2a_n = -\int_C \vec{J} \cdot \vec{E}_n^{-} dl \cdot \tag{4a}$$

On the other hand, if $\vec{E}_n^{+}$ and $\vec{H}_n^{+}$ modes are used instead,

$$2b_n = -\int_C \vec{J} \cdot \vec{E}_n^{+} dl \cdot \tag{4b}$$

Therefore the coefficients of the excited modes by the current source can be determined if only the current can be well approximated. For an SIW with equivalent width a and substrate thickness b which operates at frequencies that only TE_{10} mode propagates, the power transmitted into the SIW can be calculated by

$$P = \int_0^b \int_0^a \frac{1}{2} \mathrm{Re}\left(\vec{E}_{10} \times \vec{H}_{10}^{*}\right) \cdot \hat{a}_z \, dx \, dy \cdot \tag{5}$$

Here, the asterisk denotes complex conjugate operator. The resistive part of the equivalent input impedance, or simply the input resistance, seen from the impressed current excitation I can thus be given by

$$R_{in} = \frac{2P}{|I|^2} \cdot \tag{6}$$

It is worthy noting that the input resistance from (6) depends on the current distribution along the path C, but independent of the current magnitude.

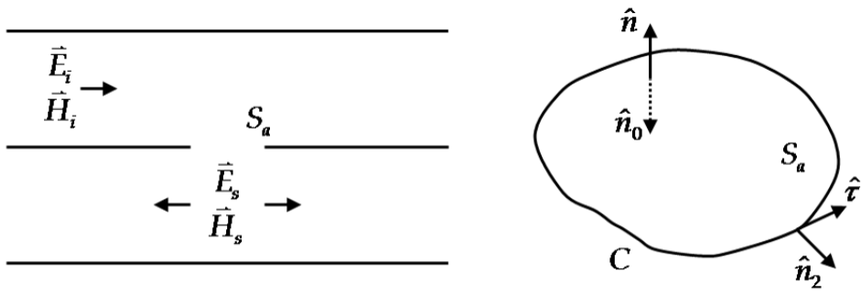

Fig. 6. (a) Waveguide excitation by slot coupling. (b) Notations on the slot aperture S_a.

2.3 Input Conductance of Slot Coupling

Waveguides can also be excited by slot coupling. Consider a small slot aperture S_a opened at the common metal wall of two waveguide structures, as shown in Fig. 6a. Incident fields $\vec{E}_i$ and $\vec{H}_i$ from the upper waveguide structure can be coupled into the lower waveguide structure through the aperture, inducing the scattered fields $\vec{E}_s$ and $\vec{H}_s$. By equivalence principle [Harrington, 2001], the aperture can be replaced by a perfect electric conductor (PEC) with properly placed magnetic current and magnetic charge.

Applying the boundary condition on the PEC, the magnetic current $\vec{J}_m$ and magnetic charge ρ_m can be determined as

$$\vec{J}_m = -\hat{n} \times \vec{E}_s, \quad \rho_m = \mu \hat{n} \cdot \vec{H}_s \cdot \tag{7}$$

However in SIWs, magnetic field usually contains only tangential component at boundary, i.e., no magnetic charge in this case. The scattered field excitation in the lower waveguide structure is contributed solely by the magnetic current. Therefore once the electric field distribution at the slot aperture is known, the equivalent magnetic current can be calculated by (7). With a similar process in 2.2, the coefficients of excited modes can be found as

$$2a_n = \int_{S_a} \vec{J}_m \cdot \vec{H}_n^- \, dS \cdot \tag{8}$$

The input power P can then be found by (5). If a voltage V is defined by integrating the electric field at input port, the input conductance can be determined by

$$G_{in} = \frac{2P}{|V|^2} \cdot \tag{9}$$

Again, the value is dependent on the voltage distribution along the slot, rather than the magnitude of the voltage.

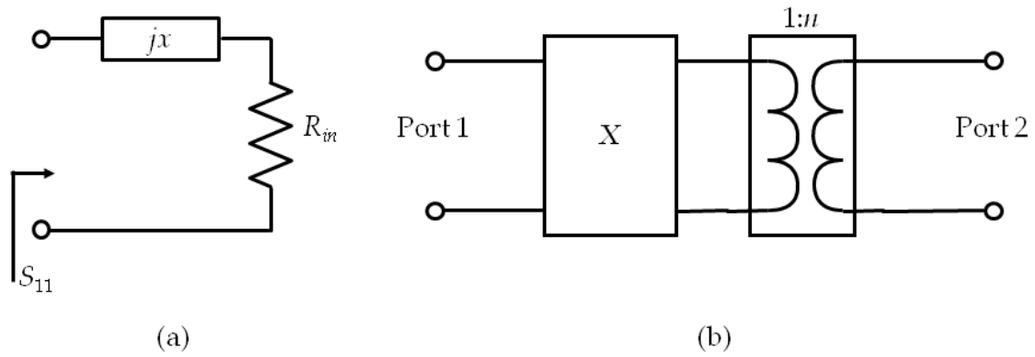

Fig. 7. (a) One port equivalent model with input resistance R_{in}. (b) Full model for the two port transition network.

2.4 Model Construction with Input Resistances

With the input resistance R is calculated in 2.2, only the reflection coefficient S_{11} at input port can be determined, as shown in Fig. 7a, where the series reactance jx is used to describe the

reactive effect which vanishes at resonance. To construct a model that can be used to determine the full scattering matrix of the two port transition network, the input resistance is replaced by a transformer with a frequency dependent ratio n determined by the calculated input resistance and the characteristic impedance of SIW. For the input conductance G_{in} calculated in 2.3, the same concept can be applied.
It should also be noted that the input port of the input resistance is defined right at the source. In practical cases additional structures are required to support the sources and usually the actual input ports are located at these structures. In general these structures are electrically small with negligible losses. Together with the series reactance jx, they can be modeled by a frequency independent reactive network $\boldsymbol{X}$. Elements in $\boldsymbol{X}$ are determined according to the physical arrangement of the structures. Since $\boldsymbol{X}$ is frequency independent, the values of its elements can be obtained by full-wave simulation at a single frequency. Figure 7b shows the full model of the two-port transition network. As will be demonstrated in the following two sections, with the frequency dependent transformer and the frequency independent reactive network, this model is able to explain the response of the transition structure over a wide frequency band.

3. MSL to SIW Transition with Shorting Via

This section proposes a transition structure between MSL and SIW by probe feeding with a shorting via. The transition structure is shown in Fig. 2. Input resistance will be calculated first according to 2.2. Transition model will then be constructed with the method discussed in 2.4. A Ka band and an E band transitions will then be demonstrated as examples.

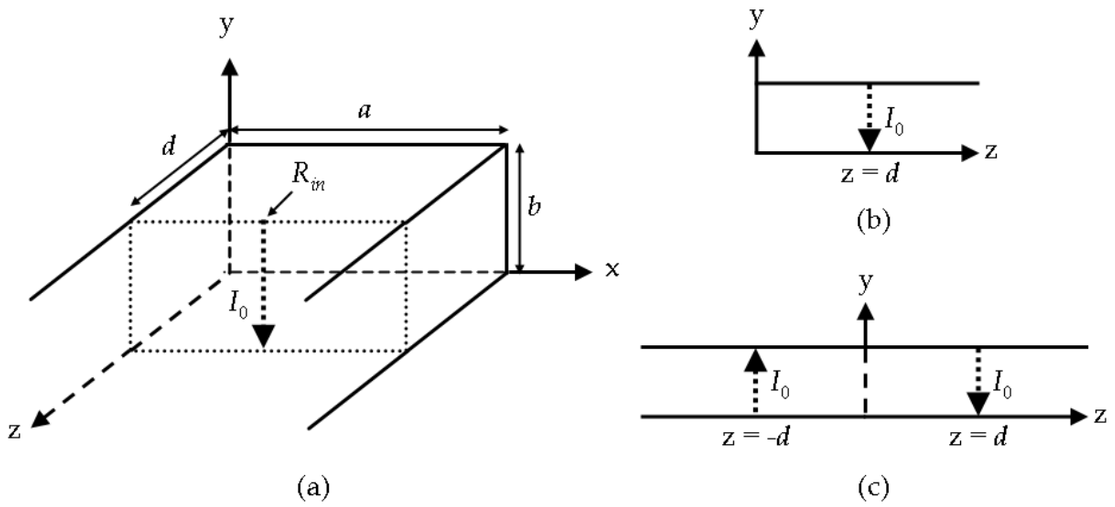

Fig. 8. Simplified problem for probe feeding. (a) Three-dimensional view. (b) Side view. (c) Side view of the equivalent problem.

3.1 Input Resistance

For a z-directed SIW with equivalent width a and substrate thickness b fed by a via probe at $z = d$, $x = a/2$, if the thickness and the via diameter are small, the current on the via can be

assumed uniformly distributed. Figure 8a shows the three-dimensional view of the simplified problem. A rectangular waveguide with one end shorted at z = 0 and the other end stretches to infinity. A linear current I_0 is used to excite the waveguide at z = d, as shown in Fig. 8b, the side view of the problem.

In order to use the theory developed in 2.2 for the calculation of input resistance R_{in}, image theory is applied to construct an equivalent problem, as shown in Fig. 8c. A rectangular waveguide with both ends stretching to infinity is excited by two opposite directed current sources with magnitude I_0 at z = ±d. Assume the only propagating mode is TE_{10}, taking a generating function from table 1 as

$$\psi_{10} = \sqrt{\frac{2}{abk\eta\beta_{10}\left(\pi/2\right)^2}} \cdot \cos\frac{\pi x}{a}, \tag{10}$$

which has been normalized to

$$\iint \vec{e}_{10} \times \vec{h}_{10}^{*} \cdot \hat{a}_z \, dx\, dy = 1 \tag{11}$$

for the convenience of power calculation. Also from table 1 the tangential field pattern of TE_{10} modes can be obtained as

$$\vec{E}_{t,10} = -jk\eta\sqrt{\frac{2}{abk\eta\beta_{10}}} \cdot \sin\frac{\pi x}{a} e^{\pm j\beta_{10}z}\hat{a}_y \tag{12a}$$

and

$$\vec{H}_{t,10} = \mp\Gamma_{10}\frac{\pi}{a}\sqrt{\frac{2a}{bk\eta\beta_{10}\pi^2}} \cdot \sin\frac{\pi x}{a} e^{\pm j\beta_{10}z}\hat{a}_x \cdot \tag{12b}$$

From (4b), coefficient of the electric field propagating in +z direction which is excited by the current I_0 at z = d can be calculated as

$$2b_1 = jI_0\sqrt{\frac{2k\eta b}{a\beta_{10}}} \cdot e^{-j\beta_{10}d} \cdot \tag{13a}$$

In the same manner, the contribution of the image current can also be determined.

$$2b_1' = -jI_0\sqrt{\frac{2k\eta b}{a\beta_{10}}} \cdot e^{j\beta_{10}d} \tag{13b}$$

Since the power flows through waveguide cross section is the combination of the power excited by the current and its image, it can be easily calculate by (5), i.e.,

$$P = \left|I_0\right|^2 \frac{kb\eta}{2a\beta_{10}} \sin^2\beta_{10}d \cdot \tag{14}$$

Therefore by (6) the input resistance can be obtained.

$$R_{in} = \frac{kb\eta}{a\beta_{10}} \sin^2\beta_{10}d \cdot \tag{15}$$

It is worthy mentioning that R_{in} reaches a maximum at $\beta_{10}d = \pi/2$, i.e., the feeding is a quarter guided wavelength from the short end of the waveguide, where the –z traveling

wave will be in phase with the +z traveling wave after reflection. As a result, maximum power can be transmitted into the waveguide.

3.2 Transition Model

After calculating the input resistance, transition model can be constructed by the procedures described in 2.4. As shown in Fig. 9a, R_{in} is the input resistance looking in to the shorting via in SIW while the actual input port is located at the MSL connecting to the via pad. It is obvious that the via pad can be viewed as a shunt capacitance C to the ground of the MSL. The inductance L in Fig. 9(b) includes the contribution from the input reactance jx, the shorted via inductance, and the inductance due to the extra via section from via pad to SIW. After replacing R_{in} by a transformer with frequency dependent ratio n, the full transition model is constructed as Fig. 9b.

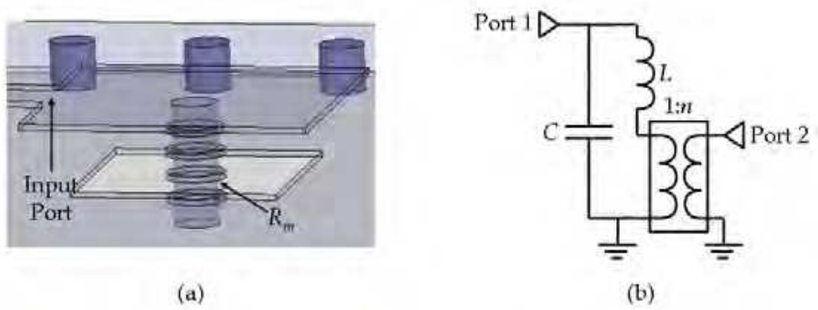

Fig. 9. Model construction according to physical structure and R_{in}. (a) Physical structure. (b) Full transition model.

In order to verify the transition model, a test transition structure was designed and simulated with Ansoft HFSS, a widely used commercial full-wave simulator. All transition structures were designed on a multilayer LTCC substrate with a relative dielectric constant 7.8 and a thickness 50.8μm for each layer. The dielectric is assumed to be lossless to simplify the investigation.

For a center frequency 30GHz, the width of SIW is chosen to be 2738μm. MSL is designed for 50Ω characteristic impedance with three layer height and 180μm width. First R_{in} is calculated separately by (15) and HFSS for different SIW heights, where in HFSS R_{in} is calculated by (6), current flows through the via is obtained by integrating the magnetic field enclosing the via and integrating the Poynting vector on SIW cross section gives power flow. Results are listed in Table 2. About 20% relative error is obtained with similar trend. This may be partly contributed to the negligence of the coupling due to the opening on the anti pad on the upper metallic wall of SIW. It can also be seen that as the height of SIW increases, the assumption of uniform current distribution in the via becomes less applicable.

SIW Layers	Formula (15)	HFSS Simulation	Relative Error
2	6.8Ω	8.1Ω	16%
4	13.6Ω	16.7Ω	18%
6	20.4Ω	25.2Ω	19%

Table 2. Input resistance with different SIW thickness by (15) and HFSS simulation.

Given the input resistance, the passive network can be adjusted for impedance matching. The main contribution of the series inductance comes from the via section above SIW, hence the adjustable range is limited. On the other hand, the value of the shunt capacitance can be easily changed by adjusting the size of the via pad and the antipad. Table 3 shows the element values tuned for the R_{in} of SIW with different layers. Size of the via pad is changed with the edge of square antipad fixed at 460μm. Also note that the closer the input resistance is to the port characteristic impedance, the wider fine tuned transition bandwidth can be obtained.

SIW Layers	R_{in} (Ω)	L (nH)	C (pF)	Viapad Size (μm)	Fractional Bandwidth
2	6.8	0.110	0.225	640	33%
4	13.6	0.118	0.17	480	43%
6	20.4	0.129	0.124	400	46%

Table 3. Element values tuned for the R_{in} of SIW with different layers and viapad sizes.

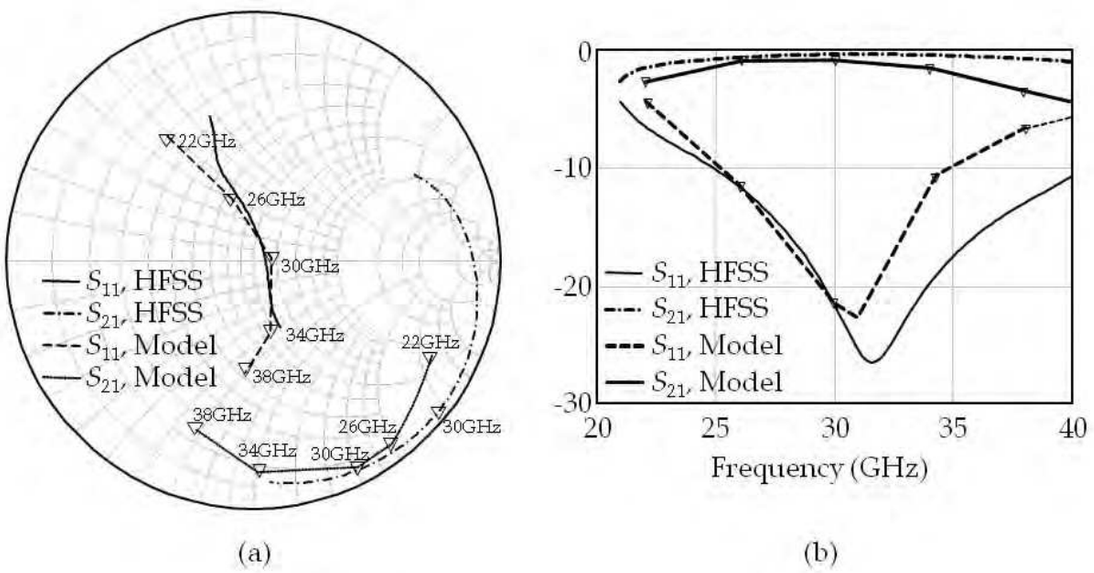

Fig. 10. Responses obtained by the shorting via transition model and HFSS. (a) Smith chart. (b) Rectangular plot.

For the test transition structure with 2-layer SIW described above, figure 10 shows the responses of the full transition model shown in Fig. 9b and the full-wave simulation results by HFSS. As can be seen, highly coherent results were obtained by the model and HFSS except a 10° phase difference in S_{21}. This may be attributed in the phase change during power transition along the via structure, which is not included in the transition model. However the model still shows its usefulness for designing MSL to SIW transitions of this type. Two practical examples were designed and fabricated on LTCC substrates, as given in the following subsections.

3.3 Ka-Band Transition Design

A transition is designed for a Ka-band transceiver module with a 31GHz center frequency, a 28-34GHz transition band for 10dB return loss and 3dB insertion loss in the back-to-back transition structure. The structure is designed on an LTCC substrate with a 7.8 relative dielectric constant and a 0.005 loss tangent at 30GHz. Thickness for each dielectric layer is 50.8μm with a 13μm silver metallization between each layer. The feeding MSL is designed for 50Ω characteristic impedance with 180μm width and 152.4μm height. The SIW is chosen to be 2738μm wide with 101.6μm thickness. Probe feeding is achieved by a shorting via located at 920μm from the shorted end of the SIW. The widths for the square viapad and antipad are 640μm and 460μm, respectively.

Figure 11a shows the simulation result by HFSS for a single transition. 9GHz bandwidth is achieved for 15dB return loss. In-band insertion loss is within 0.6dB. A back-to-back transition structure is fabricated for measurement. Figure 11b shows the comparison between simulation and measurement. As shown in the figure, 9GHz bandwidth is achieved for 10dB return loss. Insertion loss is better than 1.2dB in the entire transition band.

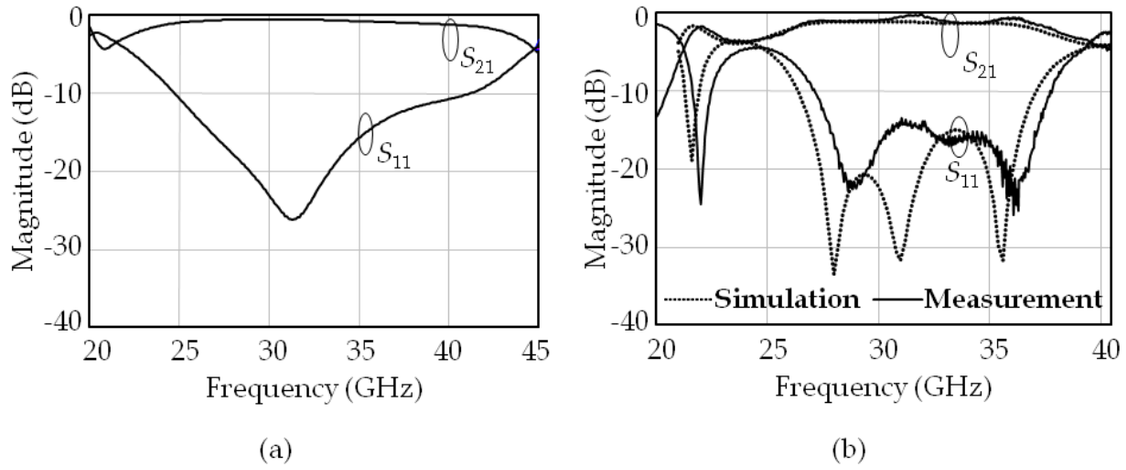

Fig. 11. Results of Ka-band MSL to SIW transition design with probe feeding by shorting via. (a) Simulation result for a single transition. (b) Comparison between simulation and measurement for the back-to-back transition.

3.4 E-Band Transition Design

Another transition is designed for an E-band transceiver module. A 73GHz center frequency is desired with a 71-76GHz transition band for 15dB return loss. The structure is designed on an LTCC substrate with a 7.8 relative dielectric constant and a 0.0078 loss tangent at 60GHz. Thickness for each dielectric layer is 50.8μm with 13μm silver metallization between each layer. The feeding MSL is designed for 50Ω characteristic impedance with 112μm width and 101.6μm height. The SIW is chosen to be 1140μm wide with 101.6μm thickness. Probe feeding is achieved by a shorting via located at 630μm from the shorted end of the SIW. The widths for the square via pad and antipad are 273μm and 373μm, respectively.

Figure 12a shows the simulation result by HFSS for a single transition. A 17% fractional bandwidth is achieved for 15dB return loss. In-band insertion loss is within 0.72dB. A back-

to-back transition structure is fabricated for measurement. Figure 12b shows the comparison between simulation and measurement, where the measured result is obtained only below 75GHz owing to equipment limitation. As shown in the figure, 13GHz bandwidth is achieved for 10dB return loss. Insertion loss is better than 2.56dB in the entire transition band.

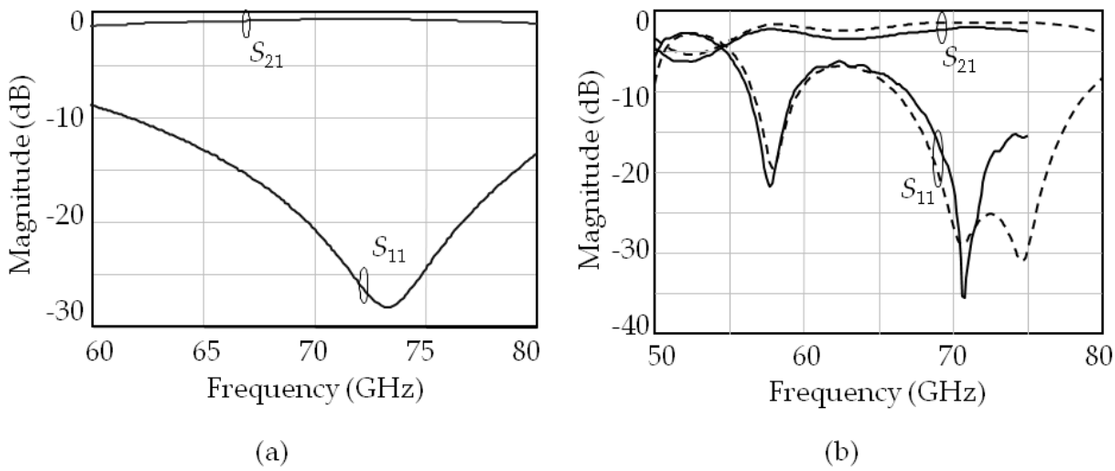

Fig. 12. Results of E-band MSL to SIW transition design with probe feeding by shorting via. (a) Simulation result for a single transition. (b) Comparison between simulation and measurement for back-to-back transition.

4. MSL to SIW Transition with Open Slot

The structure of a transition between MSL and SIW by slot coupling is shown in Fig. 3. Input conductance will be calculated first in this section followed by the construction of transition model. A Ka band and an E band transitions will also be demonstrated as examples.

4.1 Input Conductance

In contract to the probe feeding, the electric field excited by the slot is in the opposite directions for the forward and backward traveling waves. Therefore the slot should be opened as close as possible to the shorted end of the SIW to get maximum energy transfer. The transition problem can then be simplified as Fig. 13a, which shows a z-directed SIW with equivalent width a and substrate thickness b excited by a slot with length $2l$ at $z = d$. The SIW and the slot are center aligned at $x = a/2$. If the width t of the slot is small, the electric field at the slot can be assumed uniform along that direction.

In order to use the theory developed in 2.3 for the calculation of input conductance G_{in}, image theory is applied to construct an equivalent problem, as shown in Fig. 8b. A rectangular waveguide with both ends stretching to infinity is excited by two slots with the same magnetic current J_m at $z = \pm d$.

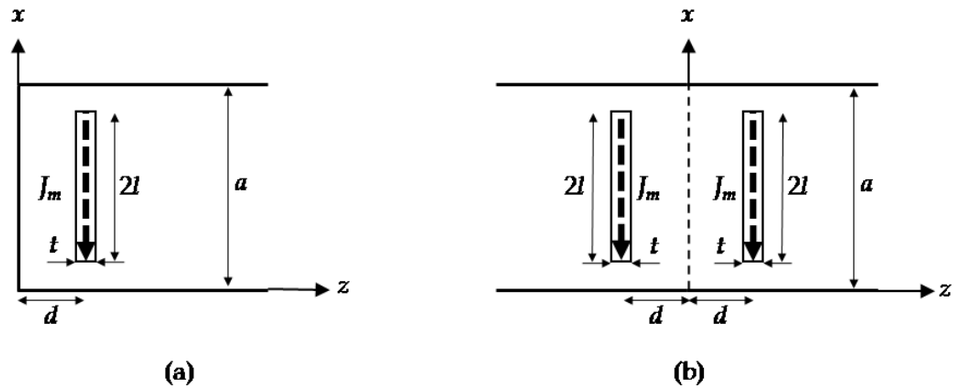

Fig. 13. (a) Top view of simplified slot coupling problem. (b) Top view of equivalent problem.

Assume the slot voltage distributes as on a slot antenna, i.e.,

$$V = V_0 \sin\left[k\left(l - \left|x - \frac{a}{2}\right|\right)\right]. \tag{16}$$

For a thin slot as described above, the electric field can be expressed as

$$\vec{E}_s = \frac{V}{t}\hat{a}_z = \frac{V_0}{t}\sin\left[k\left(l - \left|x - \frac{a}{2}\right|\right)\right]\hat{a}_z. \tag{17}$$

Therefore the magnetic current on the slot can be obtained.

$$\vec{J}_m = -\hat{n} \times \vec{E}_s = -\frac{V_0}{t}\sin\left[k\left(l - \left|x - \frac{a}{2}\right|\right)\right]\hat{a}_x. \tag{18}$$

Substitute (18) into (8) with the SIW normalized field derived in (12), the coefficient of the magnetic field propagating in +z direction which is excited by the current I_0 at z = d can be calculated as

$$2a_n = \sqrt{\frac{2}{abk\eta\beta_{10}}}\Gamma_{10}V_{10}\left(\cos k_{c,10}l - \cos kl\right)\frac{2k}{\beta_{10}^2}e^{-j\beta_{10}d}, \tag{19a}$$

On the other hand, the contribution of the image magnetic current can also be determined as

$$2a_n' = \sqrt{\frac{2}{abk\eta\beta_{10}}}\Gamma_{10}V_{10}\left(\cos k_{c,10}l - \cos kl\right)\frac{2k}{\beta_{10}^2}e^{j\beta_{10}d}. \tag{19a}$$

Power flows through waveguide cross section can then be easily calculate as

$$P = |V_0|^2 \frac{2k}{ab\eta\beta_{10}^3}\left(\cos k_{c,10}l - \cos kl\right)^2 \cos^2\beta_{10}d. \tag{20}$$

It should be noted that maximum power occurs at d = 0, i.e., the slot is opened at the shorted end of the SIW, which agrees with the discussion in the beginning of this subsection. With the calculated power flow and the defined slot voltage, the input conductance can be calculated by (9) as

$$G_{in} = \frac{4k}{ab\eta\beta_{10}^3}\left(\cos k_{c,10}l - \cos kl\right)^2 \cos^2 \beta_{10}d \cdot \tag{21}$$

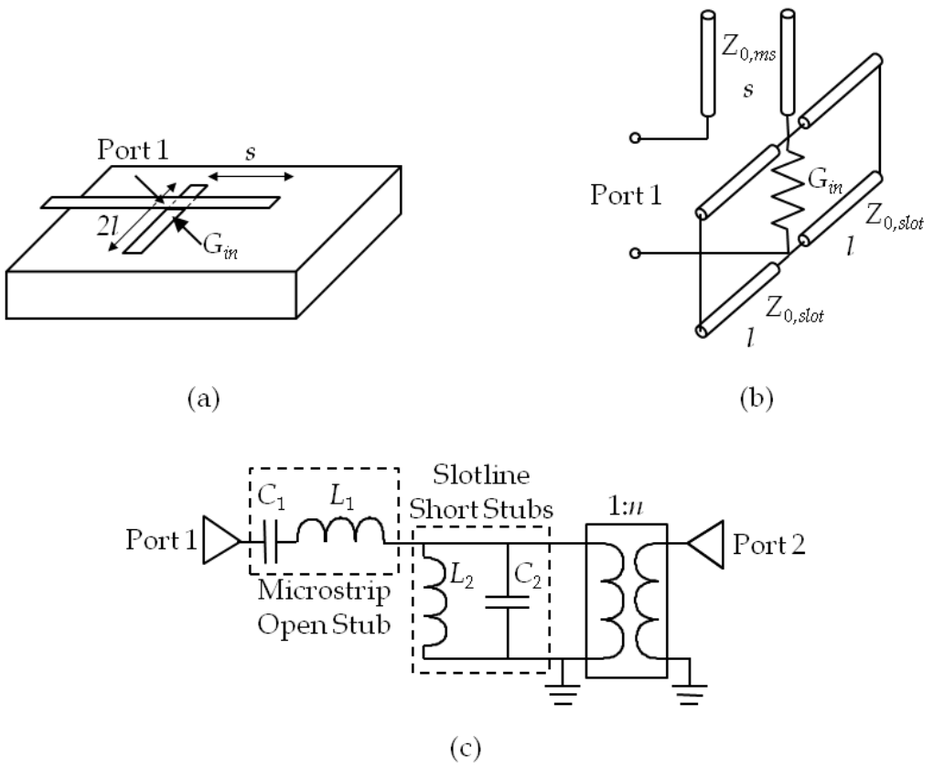

Fig. 14. Model construction for MSL to SIW transition by slot coupling. (a) Simplified transition structure. (b) Equivalent circuit using transmission line models and G_{in}. (c) Full transition model.

4.2 Transition Model

Referring to the simplified transition structure shown in Fig. 14a, G_{in} is the input conductance looking into the center of the slot on the SIW. The actual input port, i.e., Port 1, is located at the feeding MSL right above the slot. An open ended microstrip stub with length l is connected in serial with the feeding MSL. In addition, two short ended slot stubs with length $d/2$ are connected in parallel with G_{in}.

Figure 14b shows the equivalent circuit of the transition with transmission line models and G_{in}. Therefore the length for each stub can be easily determined as a quarter guided wavelength at center frequency. With these lengths, input impedance at Port 1 is equal to G_{in} at center frequency. This equivalent circuit can be further simplified around center frequency. The series microstrip open stub can be replaced by a capacitor and an inductor in serial, while the two shunt slot short stubs can be combined and replaced by a capacitor and an inductor in parallel. After replacing G_{in} by a transformer with frequency dependent ratio n, the full transition model is constructed, as shown in Fig. 14c.

A test transition structure is also designed for the verification of this model. All transition structures were designed on the same multilayer LTCC substrate with a relative dielectric

constant 7.8 and a thickness 50.8μm for each layer with lossless assumption. For a center frequency 30GHz, the width of SIW a is chosen to be 2738μm. MSL is designed for 50Ω characteristic impedance with three layer height and 180μm width. Due to the limit of fabrication process, the slot cannot be opened right at the shorted end of SIW, a minimal distance satisfying the design rules from the shorting via is used, i.e., d = 200μm.

Slot Lengths	Formula (21) (mS)	HFSS Simulation (mS)
$2l = 0.7a$	9.2	11.9
$2l = 0.8a$	12.2	14.1
$2l = 0.9a$	14.6	14.9
$2l = a$	15.6	15.9

Table 4. Input conductance by (21) and HFSS simulation for a 6-layer SIW with a slot at d = 200μm and different slot lengths $2l$ in terms of SIW width a.

SIW Layers	Formula (21) (mS)	HFSS Simulation (mS)
2	46.7	31.3
3	31.5	26.3
4	23.9	21.7
5	18.8	17.9
6	15.6	15.9

Table 5. Input conductance by (21) and HFSS simulation for SIWs with different layers with a slot at d = 200μm and slot length $2l = a$.

Instead of (21), G_{in} can also be calculated directly by (9) using HFSS, where a line integration of electric field at the center of the slot gives the slot voltage and integrating the Poynting vector on SIW cross section gives the power flow. Results for different slot length on a 6-layer SIW are shown in Table 4. As slot length increases, the input resistance decreases. It is worth mentioning that as the slot length increases toward resonance, the input resistance can be calculated by (21) more accurately. On the other hand, results for SIWs with different layers and a slot length $2l = a$ are listed in Table 5. As SIW layer increases, the input conductance decreases and the agreement with simulation results becomes better.

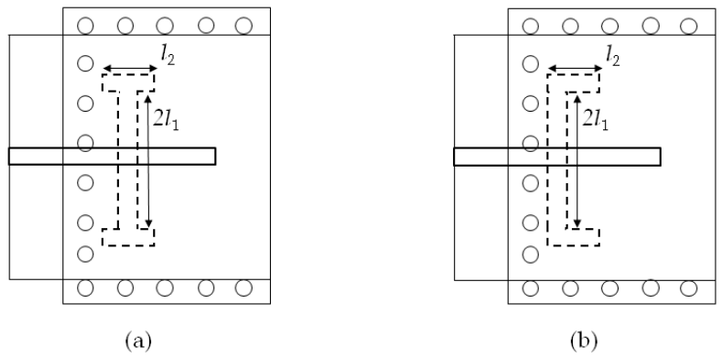

Fig. 15. Modified coupling slots. (a) H-shape slot. (b) U-shape slot.

As the transition model indicated, bandwidth is maximized for G_{in} = 1/50 Siemens. This can be achieved by adjusting the slot length for SIWs with different layers. However slot length near resonance is often desired because of maximum power transition. Therefore H-shape or

U-shape slots, as shown in Fig. 15, will be used in the following designs. In these cases, the input admittances can also be found as

$$G_{in} = \frac{4k}{ab\eta\beta_{10}^3}\left[\cos k_{c,10} l_1 \cos kl_2 - \frac{k_{c,10}}{k}\sin k_{c,10} l_1 \sin kl_2 - \cos k(l_1 + l_2)\right]^2 \cos^2 \beta_{10} d \cdot \quad (22)$$

Note that the last term in the bracket vanishes when $k(l_1+l_2)=\pi/2$, i.e., total slot length equals to half wavelength. With these kinds of slots, the effective feeding lengths of the slots can be adjusted while total slot lengths are kept near resonance.

Figure 16 shows the responses for a test transition structure with design parameters mentioned above, where 6-layer SIW is used. An H-shape slot with l_1 = 2000μm, l_2 = 600μm is opened on the SIW. Phase difference between transition model and HFSS simulation can be attributed to the phase delay during power transition, which is not included in the transition model. However the model still shows its usefulness for designing MSL to SIW transitions of this type.

As shown in Fig. 17, responses of another two transition structures are obtained. By adjusting the slot shape and length, wideband transition from MSL to SIW with different layers can be obtained. Figure 17a shows the response of transition to a 10-layer SIW by an H-shape slot with l_1 = 2500μm, l_2 = 500μm. On the other hand, Fig. 17b shows the response of transition to a 4-layer SIW by a U-shape slot with l_1 = 1100μm, l_2 = 900μm. 40% fractional bandwidth is achieved in both cases. Two practical examples were designed and fabricated on LTCC substrates, as given in the following subsections.

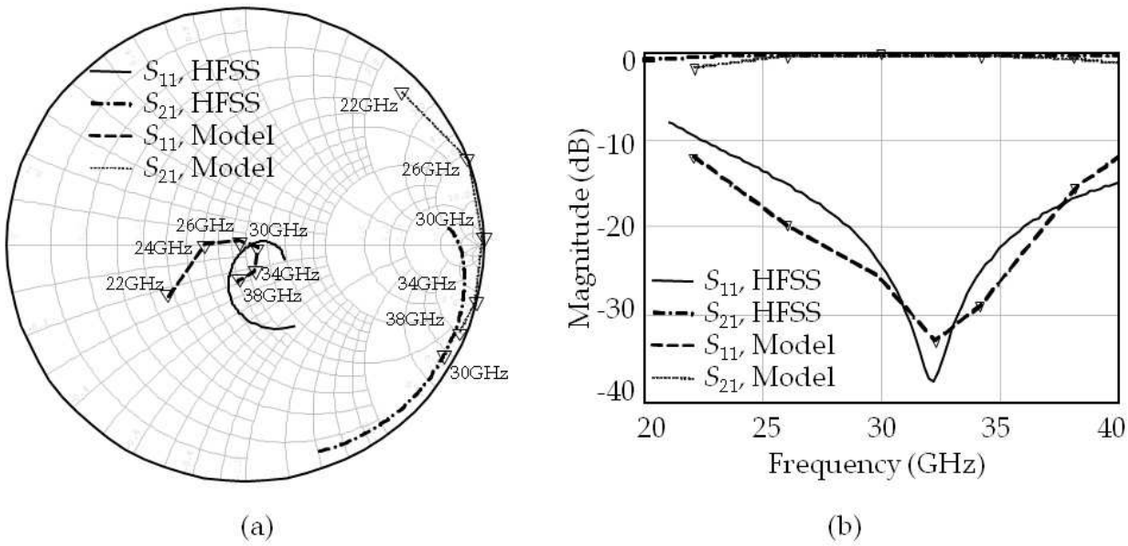

Fig. 16. Responses obtained by slot-coupled transition model and HFSS. (a) Smith chart. (b) Rectangular plot.

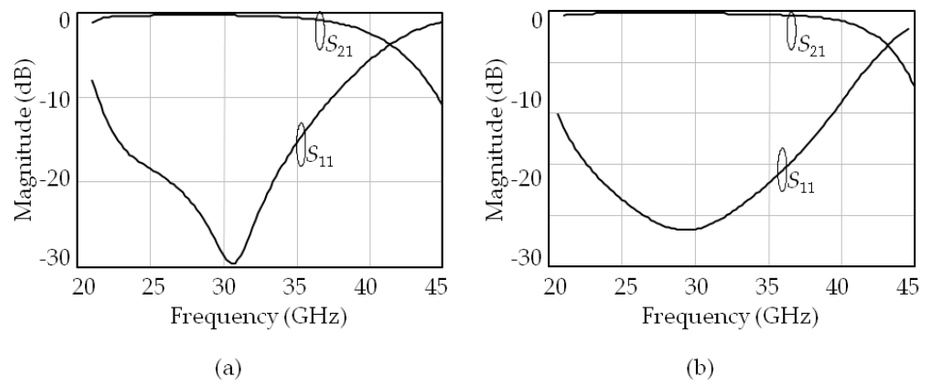

Fig. 17. Responses of slot-coupled transition with a slot at d=200μm for different slot shapes and SIW layers. (a) H-shape slot (l_1 = 2500μm, l_2 = 500μm), 10-layer SIW. (b) U-shape slot (l_1 = 1100μm, l_2 = 900μm), 4-layer SIW.

4.3 Ka-Band Transition Design

A Ka-band MSL to SIW transition by slot coupling is designed, with 31GHz center frequency, 28-34GHz transition band, 10dB return loss, and 3dB insertion loss in the back-to-back transition structure. The structure is designed on an LTCC substrate with relative dielectric constant 7.8 and loss tangent 0.005 at 30GHz. Thickness for each dielectric layer is 50.8μm with 13μm silver metallization between each layer. The feeding MSL is designed for 50Ω characteristic impedance with 180μm width and 152.4μm height. The SIW is chosen to be 2738μm wide with 304.8μm thickness. An H-shape slot with l_1 = 2000μm and l_2 = 600μm is used for the coupling.

Figure 18a shows the simulation results by HFSS for a single transition. 38% fractional bandwidth is achieved for 15dB return loss. In-band insertion loss is within 0.6dB. A back-to-back transition structure is fabricated for measurement. Figure 18b shows the comparison between simulation and measurement. As shown in the figure, more than 15GHz bandwidth is achieved for 10dB return loss. Insertion loss is better than 1.3dB in the entire transition band.

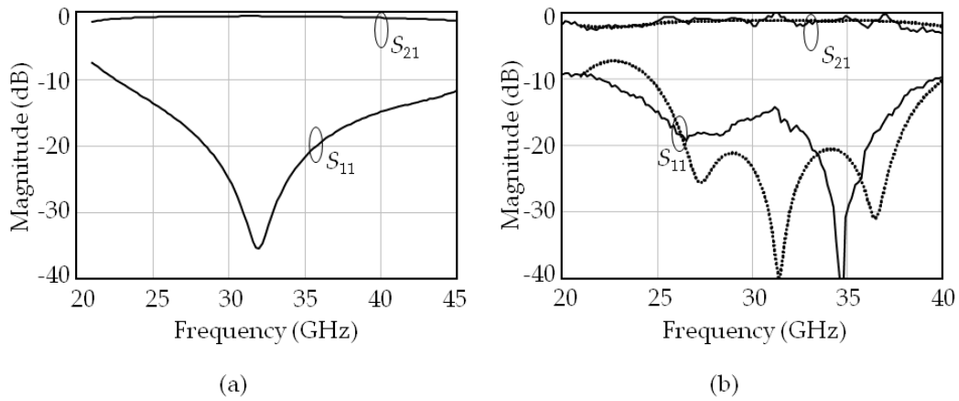

Fig. 18. Results of Ka-band MSL to SIW transition design by slot coupling. (a) Simulation result for a single transition. (b) Comparison between simulation and measurement for back-to-back transition.

4.4 E-Band Transition Design

An E-band MSL to SIW transition by slot coupling is also designed. A 73GHz center frequency is desired with 71-76GHz transition band for 15dB return loss. The structure is also designed on an LTCC substrate with relative dielectric constant 7.8 and loss tangent 0.0078 at 60GHz. Thickness for each dielectric layer is 50.8μm with a 13μm silver metallization between each layer. The feeding MSL is designed for 50Ω characteristic impedance with 112μm width and 101.6μm height. The SIW is chosen to be 1140μm wide with 203.2μm thickness. A U-shape slot with l_1 = 580μm and l_2 = 150μm is used for the coupling.

Figure 19a shows the simulation result by HFSS for a single transition. A 39% fractional bandwidth is achieved for 15dB return loss. In-band insertion loss is within 1.07dB. A back-to-back transition structure is fabricated for measurement. Figure 19b shows the comparison between simulation and measurement, where the measured result is obtained only below 75GHz owing to equipment limitation. As shown in the figure, 21GHz bandwidth is achieved for 15dB return loss. Insertion loss is better than 2.8dB in the entire transition band.

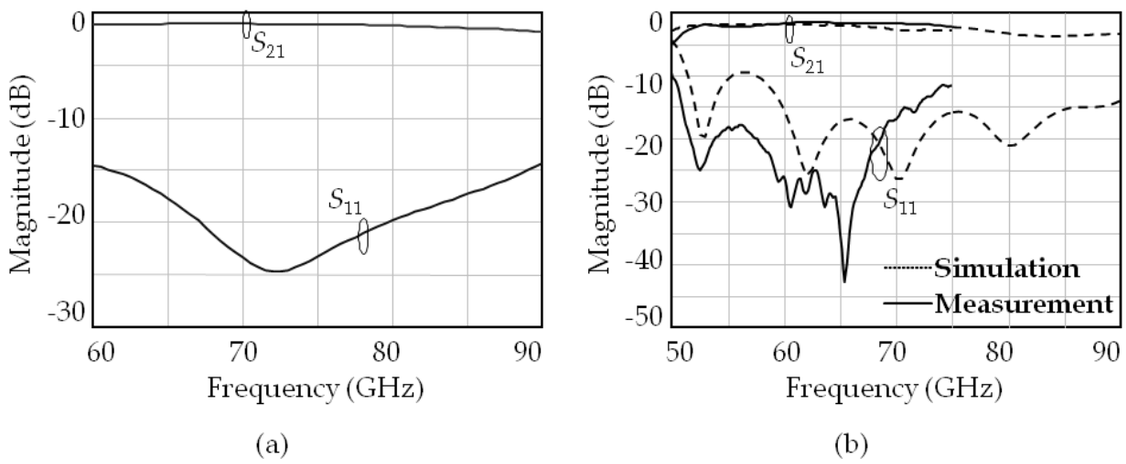

Fig. 19. Results of E-band MSL to SIW transition design by slot coupling. (a) Simulation result for a single transition. (b) Comparison between simulation and measurement for back-to-back transition.

5. Conclusions

This chapter presents systematic procedures for the design and modeling of transition structures between MSL and SIW. Input resistance or conductance of the equivalent waveguide excitation is firstly derived analytically with respect to the structural parameters of the transition. Reactive parts are then added to build the complete equivalent circuit according to the relations between voltage and current at transition discontinuities. The reactance values can be extracted by full-wave electromagnetic simulation only at center frequency. With the derived resistance and the extracted reactance values, the equivalent circuit is sufficient for wideband responses. Local compensation can then be made for maximizing the transition bandwidth. Various transition structures are designed and fabricated on LTCC substrates with center frequencies at Ka-band and E-band.

Measurements are performed on back-to-back transition structures. Good agreement between simulation and measurement results are also obtained.

For transition structures between MSL and SIW by probe feeding with a shorting via, the input resistances decrease with the thickness of SIW. Local compensation is achieved by adjusting the sizes of the via pad and the antipad. Larger transition bandwidth can be obtained for input resistances closer to the characteristic impedance of the feeding MSL. In the Ka-band designs, simulation by HFSS shows that for a single transition to SIWs with 2, 4, and 6 layers, 33%, 43%, and 46% fractional bandwidths for 15 dB return loss can be obtained, respectively. A back-to-back transition with 2-layer SIW is fabricated for measurement. Highly coherent results between simulation and measurement show that more than 30% fractional bandwidth for 10dB return loss was achieved with in band insertion loss better than 1.2dB. In the E-band design, 17% fractional bandwidth for a single transition for 15 dB return loss was obtained in HFSS simulation. Back-to-back measurement also agreed with simulation, which showed a 17% fractional bandwidth for 10dB return loss and 2.56dB in band insertion loss.

For MSL to SIW transition by slot coupling, the input conductance decreases with the thickness of SIW but increases with slot length. For different SIW layers, local compensation can be accomplished by adjusting the length and shape of the slot. Transition bandwidth can be maximized by placing the input resistances as close as to the characteristic impedance of the feeding MSL. In the Ka-band designs, simulations by HFSS show that more than 40% fractional bandwidth for 15 dB return loss can be obtained for SIWs with different layers from 4 to 10. Measurement for a fabricated back-to-back transition with 6-layer SIW agreed with simulation. More than 15GHz bandwidth for 10dB return loss was achieved with in band insertion loss better than 1.3dB. In the E-band design, 39% fractional bandwidth for 15 dB return loss was obtained in a single transition simulated by HFSS. The highly coherent results between simulation and measurement for a back-to-back structure also showed a 21GHz bandwidth for 15dB return loss. In band insertion loss is within 2.8dB. In general, the transition with slot coupling provides a wider transition bandwidth than the probe feeding.

6. References

Collins, R. E. (1991), *Field Theory of Guided Waves*, IEEE Press, ISBN: 0879422378, New York

Das, B. N.; Prasad, K. V. S. V. R.; Rao, K. V. S.; (1986). Excitation of waveguide by stripline- and mcrostrip-line-fed slots, *IEEE Trans. Microw. Theory Tech.*, Vol. 34, No. 3, Mar. 1986, pp. 321-327, ISSN: 0018-9480

Deslandes, D. & Wu, K. (2001a). Integrated microstrip and rectangular waveguide in planar form, *IEEE Microw. Wireless Compon. Lett.*, Vol. 11, No. 2, Feb. 2001, pp. 68-70, ISSN: 1531-1309

Deslandes, D. & Wu, K. (2001b). Integrated transition of coplanar to rectangular waveguide, *IEEE MTT-S Intl. Microw. Symp. Dig.*, Vol. 2, pp. 619-622, ISBN: 0780365380, Phoenix, USA, May 2001

Grabherr, W.; Huder, B. & Menzel, W. (1994). Microstrip to waveguide transition compatible with MM-wave integrated circuits, *IEEE Trans. Microw. Theory Tech.*, Vol. 42, No. 9, Sept. 1994, pp. 1842-1843, ISSN: 0018-9480

Harrington, R. F. (2001). *Time-Harmonic Electromagnetic Fields*, 2nd ed., IEEE Press, ISBN: 047120806X, New York

Huang, Y.; Wu, K. L. & Ehlert, M. (2003). An integrated LTCC laminated waveguide to microstrip line T-junction, *IEEE Microw. Wireless Compon. Lett.*, Vol. 13, No. 8, Aug. 2003, pp. 338-339, ISSN: 1531-1309

Kaneda, N.; Qian, Y. & Itoh, T. (1999). A broad-band microstrip-to-waveguide transition using quasi-Yagi antenna, *IEEE Trans. Microw. Theory Tech.*, Vol. 47, No. 12, Dec. 1999, pp. 2562-2567, ISSN: 0018-9480

Kai, T.; Hirokawa J.; Ando, M.; Nakano H. & Hirachi Y. (2005). Coaxial-line feed for post-wall waveguide in millimeter wave band, *Proc. 2005 IEEE AP-S Intl. Symp.*, pp.631-634, vol. 1A, Washington D.C., USA, July 2005.

Liang, J.-F.; Chang, H.-C. & Zaki, K. A. (1992). Coaxial probe modeling in waveguides and cavities, *IEEE Trans. Microw. Theory Tech.*, Vol. 40, No. 12, Dec. 1989, pp. 2172-2180, ISSN: 0018-9480

Lin, T.-H. & Wu, R.-B. (2001). CPW to waveguide transition with tapered slotline probe, *IEEE Microw. Wireless Compon. Lett.*, Vol. 11, No. 7, July 2001, pp. 314-316, ISSN: 1531-1309

Rollins, J. M. & Jarem, J. M. (1989). The input impedance of a hollow-probe-fed, semi-infinite rectangular waveguide, *IEEE Trans. Microw. Theory Tech.*, Vol. 37, No. 7, July 1989, pp. 1144-1146, ISSN: 0018-9480

Shih, Y. C.; Ton, T. N & Bui, L. Q. (1998). Waveguide-to-microstrip transitions for millimeter-wave applications, *IEEE MTT-S, Intl. Microw. Symp. Dig.*, Vol. 1, pp. 473-475, ISBN: 0780344715, Baltimore, USA, May 1998

Uchimura, H.; Takenoshita, T. & Fujii, M. (1998). Development of a laminated waveguide, *IEEE Trans. Microw. Theory Tech.*, Vol. 46, No 12, Dec. 1998, pp. 2438-2443, ISSN: 0018-9480

Valois, R.; Baillargeat, D.; Verdeyme, S.; Lahti, M. & Jaakola, T. (2005). High performances of shielded LTCC vertical transitions from DC up to 50 GHz, *IEEE Trans. Microw. Theory Tech.*, Vol. 53, No. 6, Jun. 2005, pp. 2026-2032, ISSN: 0018-9480

Yang, T.-H.; Chen, C.-F.; Huang, T.-Y.; Wang, C.-L. & Wu, R.-B. (2005). A 60GHz LTCC transition between microstrip line and substrate integrated waveguide, *Proc. 2005 Asia Pacific Microw. Conf.*, Vol. 1, pp. 4-7, Suzhou, China, Dec. 2005

Yau, C.-K.; Huang, T.-Y.; Shen, T.-M.; Chien, H.-Y. & Wu, R.-B. (2007). Design of 30GHz transition between microstrip line and substrate integrated waveguide, *Proc. 2007 Asia Pacific Microw. Conf.*, Bangkok, Thailand, Dec. 2007

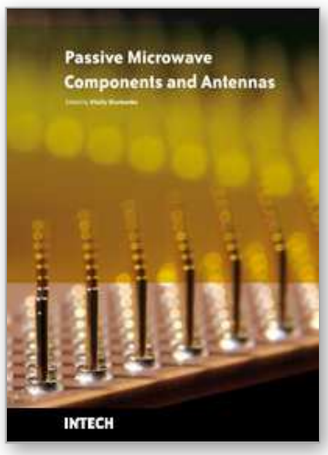

Passive Microwave Components and Antennas

Edited by Vitaliy Zhurbenko

ISBN 978-953-307-083-4
Hard cover, 556 pages
Publisher InTech
Published online 01, April, 2010
Published in print edition April, 2010

Modelling and computations in electromagnetics is a quite fast-growing research area. The recent interest in this field is caused by the increased demand for designing complex microwave components, modeling electromagnetic materials, and rapid increase in computational power for calculation of complex electromagnetic problems. The first part of this book is devoted to the advances in the analysis techniques such as method of moments, finite-difference time- domain method, boundary perturbation theory, Fourier analysis, mode-matching method, and analysis based on circuit theory. These techniques are considered with regard to several challenging technological applications such as those related to electrically large devices, scattering in layered structures, photonic crystals, and artificial materials. The second part of the book deals with waveguides, transmission lines and transitions. This includes microstrip lines (MSL), slot waveguides, substrate integrated waveguides (SIW), vertical transmission lines in multilayer media as well as MSL to SIW and MSL to slot line transitions.

How to reference

In order to correctly reference this scholarly work, feel free to copy and paste the following:

Ting-Yi Huang, Tze-Min Shen and Ruey-Beei Wu (2010). Design and Modeling of Microstrip Line to Substrate Integrated Waveguide Transitions, Passive Microwave Components and Antennas, Vitaliy Zhurbenko (Ed.), ISBN: 978-953-307-083-4, InTech, Available from: http://www.intechopen.com/books/passive-microwave-components-and-antennas/design-and-modeling-of-microstrip-line-to-substrate-integrated-waveguide-transitions

INTECH
open science | open minds

InTech Europe
University Campus STeP Ri
Slavka Krautzeka 83/A
51000 Rijeka, Croatia
Phone: +385 (51) 770 447
Fax: +385 (51) 686 166
www.intechopen.com

InTech China
Unit 405, Office Block, Hotel Equatorial Shanghai
No.65, Yan An Road (West), Shanghai, 200040, China
中国上海市延安西路65号上海国际贵都大饭店办公楼405单元
Phone: +86-21-62489820
Fax: +86-21-62489821

© 2010 The Author(s). Licensee IntechOpen. This chapter is distributed under the terms of the Creative Commons Attribution-NonCommercial-ShareAlike-3.0 License, which permits use, distribution and reproduction for non-commercial purposes, provided the original is properly cited and derivative works building on this content are distributed under the same license.

IntechOpen

IntechOpen